HHS Public Access

Author manuscript

Traffic. Author manuscript; available in PMC 2024 January 01.

Published in final edited form as:

Traffic. 2023 January ; 24(1): 4–19. doi:10.1111/tra.12873.

Cab45 deficiency leads to the mistargeting of progranulin and prosaposin and aberrant lysosomal positioning

Mai Ly Tran[1], **Johanna Tüshaus**[2,3], **Yeongho Kim**[1], **Bulat R. Ramazanov**[1], **Swathi Devireddy**[1,4,5,6], **Stefan F. Lichtenthaler**[2,3,7], **Shawn M. Ferguson**[1,4,5,6], **Julia von Blume**[1,†]

[1]Department of Cell Biology, Yale University School of Medicine, New Haven, CT, USA

[2]German Center for Neurodegenerative Diseases (DZNE), Munich, Germany

[3]Neuroproteomics, School of Medicine, Klinikum Rechts der Isar, Technical University of Munich, 81675

[4]Department of Neuroscience, Yale University School of Medicine, New Haven, CT, USA

[5]Program in Cellular Neuroscience, Neurodegeneration and Repair, Yale University School of Medicine, New Haven, CT, USA

[6]Wu Tsai Institute, Yale University, New Haven, CT, USA

[7]Munich Cluster for Systems Neurology (SyNergy), Munich, Germany

Abstract

The trans-Golgi Network (TGN) sorts molecular “addresses” and sends newly synthesized proteins to their destination via vesicular transport carriers. Despite the functional significance of packaging processes at the TGN, the sorting of soluble proteins remains poorly understood. Recent research has shown that the Golgi resident protein Cab45 is a significant regulator of secretory cargo sorting at the TGN. Cab45 oligomerizes upon transient Ca^{2+} influx, recruits soluble cargo molecules (clients), and packs them in sphingomyelin-rich transport carriers. However, the identity of client molecules packed into Cab45 vesicles is scarce. Therefore, we used a precise and highly efficient secretome analysis technology called hiSPECs. Intriguingly, we observed that Cab45 deficient cells manifest hypersecretion of lysosomal hydrolases. Specifically, Cab45 deficient cells secrete the unprocessed precursors of prosaposin (PSAP) and progranulin (PGRN). In addition, lysosomes in these cells show an aberrant perinuclear accumulation suggesting a new role of Cab45 in lysosomal positioning. This work uncovers a yet unknown function of Cab45 in regulating lysosomal function.

[†]Corresponding author: Julia von Blume, julia.vonblume@yale.edu, Phone: +1 475 325 8124.

Author Contributions

SFL and JT performed the MS experiments and provided unlimited support; MLT has conducted the experiments. SMF shared valuable reagents and his expertise in the field. SD provided the PSAP-mCherry RUSH construct, SORT1KO cells, and CI-M6PRKO cells. YK supported us with the live cell imaging RUSH experiments. BR performed qRT-PCR experiments and DQ-BSA assays. MLT and JVB conceived the project, designed experiments, analyzed data, and wrote the manuscript.

Declaration of Interest

The authors declare no conflict of interest.

Keywords

TGN export; Cab45; lysosomal hydrolases; prosaposin; progranulin

Introduction

Soluble secreted proteins, including lysosomal enzymes, are introduced into the endoplasmic reticulum (ER) via their signal sequence (Lingappa and Blobel, 1980). In the ER, they are folded and transported from the ER lumen to the Golgi apparatus (GA) in COPII-coated vesicles (Miller and Barlowe, 2010). The proteins move from cis, medial to the trans-Golgi and then to the trans-Golgi Network (TGN). In the TGN, cargo proteins are sorted into specific transport carriers, which direct them to the endolysosomal system or the cell surface for secretion. (Stalder and Gershlick, 2020; Mostov and Cardone, 1995; Tang, 2001). Understanding the sorting of these molecules in the TGN lumen is challenging since luminal molecules require mechanisms of membrane recruitment to facilitate the budding of a carrier (Ramazanov et al., 2021; Kienzle and von Blume, 2014).

The sorting and packaging of luminal lysosomal hydrolases in the TGN occur by cargo receptors in the TGN membrane (Ghosh et al., 2003). These receptors include the cation-dependent (CD) and the cation-independent (CI) mannose-6-phosphate receptor (MP6R) or sortilin1 (Yang and Wang, 2021; Braulke and Bonifacino, 2009). The luminal domains of these sorting receptors recognize either a specific glycan modification, such as N-linked mannose-6-phosphate (M6PR), or a folded polypeptide sequence displayed on the hydrolase surface (Saftig and Klumperman, 2009; Kienzle and von Blume, 2014). Sortilin (SORT1) binds to these peptide ligands via a tunnel-like structure formed by the VPS10p β-propeller domain in the TGN (Quistgaard et al., 2009) (Saftig and Klumperman, 2009; Coutinho et al., 2012). The cytosolic domains of the receptors bind to adaptor proteins such as Golgi-localized, γ-ear–containing, ARF-binding proteins or adaptor protein 1 complex that recruit coat proteins to form clathrin-coated vesicles targeted to endolysosomes (Puertollano et al., 2001; Klumperman et al., 1993; Doray et al., 2002; Saftig and Klumperman, 2009; Bajaj et al., 2019). If the recognition of the lysosomal proteins by their receptors in the TGN lumen fails, the precursor proteins are secreted from cells (reviewed in Saftig and Klumperman, 2009). Impaired lysosomal targeting of these hydrolases causes defective degradation of proteins and lipids, which accumulate in lysosomes leading to lysosomal storage diseases (Zhang et al., 2021, Tayebi et al., 2020).

Prosaposin (PSAP) and progranulin (PGRN) are lysosomal hydrolases required to maintain normal lysosome function (Zhang et al., 2022; Kim et al., 2022). The sorting of PSAP and PGRN into the correct vesicular carrier, targeting them to the lysosome, is crucial for their function. PSAP precursors mature in the lysosome to Saposin A-D required for glycosphingolipid degradation (O'Brien and Kishimoto, 1991). PGRN is processed into granulin peptides that regulate the activity of several lysosomal enzymes, such as cathepsin D (Zhou et al., 2017 (2). The loss of function of these enzymes has been linked to neurodegenerative diseases (Tayebi et al., 2020). The CI-M6PR sorts PSAP from the TGN to the endolysosomal system (Nicholson et al., 2016; Zhou et al., 2015). Likewise, sortilin

sorts PGRN in the TGN. Alternatively, prosaposin interacts with progranulin and links it to the CI-M6PR (Nicholson et al., 2016; Zhou et al., 2015). Sortilin and CI-M6PR also bind these hydrolases for endocytic uptake (Gopalakrishnan et al., 2004; Laurent-Matha et al., 2002; Zhou et al., 2017 (3); Tayebi et al., 2020). As these sorting processes are redundant, it has been challenging to identify significant molecular interactions facilitating PSAPs' and PGRNs' correct transport to lysosomes.

Cab45 regulates the export of secretory proteins from the TGN. Cab45 is a low-affinity Ca^{2+} binding protein with 6 EF-hand domains localized in the Golgi lumen (Scherer et al, 1996). In the presence of Ca^{2+}, Cab45 oligomerizes and captures secretory proteins (clients) and packs them into sphingomyelin-rich vesicles targeted to the cell surface (Deng et al., 2018, Crevenna et al., 2016). Here we analyzed the secretome of control and Cab45 deficient cells by iSPECS. Our results show that Cab45 deficiency leads to the secretion of the inactive precursors of PRGN and PSAP, suggesting a fundamental role of Cab45 in facilitating the sorting of these proteins to lysosomes. Intriguingly, Cab45-deficient cells show an aberrant perinuclear accumulation of lysosomes pinpointing an essential role of Cab45 in lysosomal positioning. In summary, we propose an unexpected new role of Cab45 in lysosomal biology.

Results and Discussion

Identification of novel Cab45 clients

We previously demonstrated that Cab45 recruits a subset of client molecules in the TGN and that the absence of Cab45 impaired the secretion of these molecules (von Blume et al., 2012, Crevenna et al., 2016, Deng et al., 2018). Thus, this study aimed to identify a broader class of Cab45 clients to gain insight into the binding mechanism by grouping these into functional categories and possibly identifying conserved binding motifs. Accordingly, we performed high-performance secretome protein enrichment with the click sugars (hiSPECS) method (Kuhn et al., 2012; Tüshaus et al., 2020) to compare secreted proteins in control or Cab45 siRNA-treated HeLa cells, respectively (Figure 1A). This method allows analysis of cell secretomes in the presence of serum from cellular media, thereby avoiding starvation effects. By adding N-azido-acetyl-mannosamine-tetracylated (Ac4ManNAZ) labeling sugars in the growth media of cells, newly synthesized proteins gain an amine-linked mannose modification for labeling glycosylated proteins.

We collected cells and cell culture supernatants 48 h after treatment with control or Cab45 siRNA. Cellular debris was removed by filtration of cell culture supernatants for a subsequent *in vitro* click reaction of labeled glycoproteins to DBCO-magnetic beads (Tüshaus et al., 2020). Peptides were generated by on-bead trypsinization and analyzed by mass spectrometry (MS, Figure 1A). The Cab45 knockdown was confirmed by quantitative real-time polymerase chain reaction (qRT-PCR) and western blotting (Figure 1B, Figure 1C, D). The hiSPECS results are presented in a volcano plot (Figure 1E) with the threshold set below 2log. The left side of the volcano plot depicts proteins that show reduced secretion in Cab45-deficient cells compared to control cells. Proteins secreted less efficiently from Cab45-deficient cells could not be grouped according to specific features such as structural elements, linear binding motifs, or sequence conservation (von Blume et al., 2009, 2011).

In contrast, we found a class of proteins that were hypersecreted from Cab45 depleted cells compared to control cells (right-hand side of the volcano plot). Surprisingly, 70 % of these proteins were secreted lysosomal hydrolases (Figure 1E, highlighted in pink, Table S1). This result was intriguing as our former work has shown that depletion of ADF/cofilin, treatment with F-actin modulating drugs, and SPCA1 and Cab45 deficiency induced the hypersecretion of cathepsin D (CatD) (von Blume, 2011, 2012). In this context, it is also important to note that in yeast ts-cof1-and pmr1-deletion mutants (ts-cof1 is a temperature-sensitive cofilin mutant, pmr1 is the orthologue of SPCA1), carboxypeptidase Y, a soluble vacuolar hydrolase, is missorted and hypersecreted (Curwin et al., 2012; Crevenna et al., 2016; von Blume et al., 2012; 2011; 2009; Okreglak and Drubin, 2007). These observations implied a novel function of Cab45 independent of the recently described client-clustering mechanism that sorts clients into sphingomyelin-rich transport carriers (Crevenna et al., Deng et al.). These results suggested that Cab45 significantly impacts the TGN export of lysosomal hydrolases.

Cab45-deficient cells hypersecrete PSAP AND PGRN

We selected two candidates of interest for validation: PSAP and PGRN (Figure 1E). PSAP and PGRN are binding partners helping each other's recognition by CI-M6PR as well as the SORT1 receptor (Zhou et al. 2015; 2017 (1), (2)). To validate the role of Cab45 in the hypersecretion of PSAP and PGRN, we performed secretion assays to identify secreted endogenous proteins from HeLa cells. To this end, we collected cell culture supernatants from control and Cab45 siRNA-treated cells and analyzed them by SDS-PAGE and western blotting. Our results confirmed a significantly higher abundance of PSAP and PGRN proteins in cell culture supernatants collected from Cab45-deficient compared to control cells after 24 hours of incubation in an FCS-free medium (Figure 2A and 2B). Furthermore, we observed that these cells released the immature precursors of PSAP (80 kD) and PRGN (75 kD), substantiating their missorting from the TGN (Pérez-Victoria et al., 2008). Next, to further substantiate our results, we performed immunoprecipitation experiments of PSAP from control and Cab45 deficient cells incubated in FCS-containing media for 2 and 4 h. We observed a significant time-dependent increase of PSAP abundance in the medium of Cab45 deficient cells (Figure 2C, D).

To further exclude the possibility that hypersecretion is caused by higher expression of PSAP and PGRN in Cab45 depleted cells, we analyzed transcript levels of the respective proteins by qRT-PCR (Figure S1A). Our results demonstrated an equal abundance of PSAP mRNA levels in HeLa wild-type (wt), control siRNA, and Cab45 siRNA-treated cells (Figure S1B left). At the same time, the quantity of PGRN mRNA was lower in control and Cab45 siRNA-treated cells. These results validated that Cab45 deficient cells hypersecrete PSAP and PGRN.

Cab45 depletion enhances the hypersecretion of PSAP from CI-M6PR KO cells

We next tested the influence of the absence of the well-established cargo receptors of PSAP and PGRN on their secretion (Figure 3A, left). CI-M6PR interacts with PSAP via its M6P-modification, while SORT1 recognizes and sorts PGRN (Zhou et al., 2015, Qian et al., 2008). However, it has also been shown that both hydrolases can piggyback each other to be

targeted into vesicular carriers towards lysosomes (Zhou et al., 2017 (1), Zheng et al., 2011, Wahe et al., 2010). Therefore, we performed secretion assays to test how the KO of either SORT1 or CI-M6PR impacts their lysosome targeting. To this end, we incubated control, SORT1, and CI-M6PRKO cells (cartoon, Figure 3A, right) with a serum-free medium and assessed PSAP and PRGN abundance in cells and media. Interestingly, the loss of either CI-M6PR or SORT1 had no impact on PSAP secretion. The loss of SORT1 leads to a modest but significant increase in PGRN secretion. These results showed that removing the PSAP and PRGN receptors does not dramatically increase their secretion, further emphasizing the significance of the Cab45-dependent hypersecretion phenotype (Figures 3B and 3C).

To investigate if Cab45 impacts the secretion of PSAP and PGRN in CI-M6PR or SORT1KO cells, we depleted Cab45 in these cells. Western blotting of cell lysates and media showed that Cab45 depletion had no additional impact on PSAP and PGRN secretion in SORT1KO cells (Figure 3F, G). In contrast, in CI-M6PRKO cells, Cab45 lack led to a significant (2-fold and 3.5-fold) increase in PSAP and PGRN abundance in cell culture supernatants (Figure 3D, E). These increases were higher than the 1.3-fold increase observed for PSAP and PGRN secretion in HeLa cells treated with Cab45 siRNA compared with cells treated with control siRNA (Figure 2B). Therefore, we concluded that the depletion of M6PR and Cab45 enhanced the hypersecretion defect suggesting that M6PR and Cab45 may act synergistically.

Insufficient retrieval of extracellular PSAP or PGRN from the cell surface could be an alternative explanation for increased PSAP levels in cell supernatants (Bajaj et al., 2018). To exclude that Cab45 deficiency changes the retrieval of extracellular PSAP or PRGN from the cell surface, we compared the cell surface expression of CI-M6PR using cell surface biotinylation experiments. Three independent results showed no difference in CI-M6PR surface expression in control versus Cab45KO cells (Figure S1B).

Taking into account the complexity of pathways by which PSAP reaches lysosomes and the influence of Cab45 depletion in cells deprived of CI-M6PR, we hypothesize that Cab45 supports the binding of lysosomal receptors to PSAP. Alternatively, it could promote the piggybacking of PGRN and PSAP binding to their respective receptors.

Depletion of Cab45 resulted in increased TGN export of PSAP.

Our work suggested that Cab45 is involved in the cargo-receptor-dependent capture of lysosomal hydrolases. How does the Cab45 depletion affect PSAP trafficking? We used the Retention-Using-Selective-Hooks (RUSH) system (Figure S2A) to test this. A synchronized release of the fluorophore-labeled protein of interest from the ER and subsequent compartments of the secretory pathway upon biotin addition (Boncompain et al., 2012).

To determine the role of Cab45 in PSAP trafficking, we analyzed the kinetics of TGN export of RUSH-PSAP in cells expressing BFP-GalT1 (trans-Golgi marker) (Experimental workflow in Figure 4A). The TGN export rates were determined by analyzing the decrease of PSAP-mCherry fluorescence intensity (mean F.I.) in the BFP-GalT1 positive area in control and Cab45KO HeLa cells, respectively (Figure 4C). PSAP micrographs in HeLa

and Cab45KO cells depict PSAP localization in the ER before biotin addition, in the trans-Golgi after biotin addition (peak F.I.), and in budding and post-Golgi vesicles (Figure 4B). For quantification, we plotted the peak F.I. of PSAP-mCherry in the trans-Golgi at t = 0 after biotin addition and measured the decay of F.I. in control and Cab45KO cells (Figure 4D, blue). The exponential decay of PSAP-mCherry from TGN in Cab45KO cells was significantly enhanced compared to control cells. To show the specificity of elevated TGN exit of PSAP in Cab45KO cells, we performed rescue experiments using Cab45KO cells stably expressing Cab45wt (Crevenna et al., 2016; Figure 4D, yellow). The course of the exponential decay was similar to that seen in HeLa cells, indicating a successful rescue. We measured the half-life of the decline by reading the time points from three independent experiments (Figure S2B), at which 50% of the maximal F.I. of PSAP-mCherry was reached (Figure 4E). The shortest half-life of PSAP was obtained from Cab45KO cells (11.24 min), with a longer half-life in both HeLa and Cab45wt rescue cells (15.46 min, and 14.85 min, respectively).

Next, we asked if the Cab45-dependent PSAP trafficking depends on the Ca^{2+}-binding ability of Cab45 (Crevenna et al., 2016). We analyzed trans-Golgi exit of RUSH PSAP-mCherry in Cab45KO cells stably expressing a Ca^{2+}-binding deficient mutant of Cab45 (Cab45-6EQ, Crevenna, et al., 2016) (Figure 4D, green, E). We found that expression of the Cab45-6EQ mutant leads to a decrease in half-life like that in Cab45KO cells (Figure 4E). In summary, our results demonstrate that the loss of Cab45 leads to an accelerated TGN export of PSAP. We anticipate that export acceleration is the consequence of a reduced binding and capturing of PSAP by receptors. The effect is specific as the expression of the wild-type protein but not the inactive Cab45 mutant rescues the defect. This demonstrates a new function of Cab45 that involves capturing specific lysosomal hydrolases in the trans-Golgi, influencing their abundance in lysosomes.

Cab45-deficient cells accumulate perinuclear LAMP1-positive lysosomes.

Trafficking experiments showed an increase in the export of PSAP in Cab45-deficient cells. If CI-M6PR is absent, these enzymes are not efficiently transported to lysosomes and are thus secreted from cells. Former work has shown that missorting of PGRN and PSAP significantly impacts lysosome homeostasis (Evers et al., 2017; Ni et al., 2006; Tayebi et al., 2020). Thus, we hypothesized that Cab45 deficiency might impact lysosome morphology and organization. To test the hypothesis, we visualized lysosomes in control and Cab45KO cells using immunofluorescence microscopy using a LAMP1 antibody (Figure 5A). In line with previously published results, we show that LAMP1 co-localizes with PSAP and is an optimal marker for evaluating lysosomes in control and Cab45KO cells (Devireddy and Ferguson, 2022, Figure 5C, Figure S3D).

In control cells, LAMP1 appears as spherical structures that are mostly dispersed throughout the cell (termed peripheral) (Cheng et al., 2017). However, intriguingly, we observed that anti-LAMP1 signals in Cab45KO cells manifested an accumulation of LAMP1-positive lysosomes in the perinuclear region. However, the size and structure of individual lysosomes were not altered in control versus Cab45KO cells. To quantify this phenotype, we manually selected the area as a region of interest covered by the LAMP1 signal intensity and

divided this by the total area of each cell as described in (Devireddy and Ferguson, 2022). There was a significantly higher number of cells with a high percentage of LAMP1 area coverage (peripheral) for HeLa cells compared with that in Cab45KO cells (mean LAMP1 area coverage: 52.43% and 33.37%, respectively) (Figure 5B). Next, we analyzed the localization of endogenous PSAP related to LAMP1-positive structures in HeLa wt and Cab45KO cells (Figure 5C). Pearson's correlation coefficients showed a significantly reduced co-localization of PSAP and LAMP1 in Cab45 deficient cells, confirming that there is less PSAP in lysosomes of Cab45 deficient cells. Re-expression of Cab45wt rescued the overlap of PSAP with LAMP1, while the Ca^{2+} binding deficient Cab45 mutant failed to do so (Figure 5C, 5D).

We determined the localization of RUSH-PSAP mCherry in control and Cab45 deficient cells after 3 hours of biotin incubation. Our results showed that the PSAP structures are near LAMP1. However, there is no complete overlap between the two markers in control and Cab45KO cells, as observed by analyzing the endogenous proteins (Figure 5C, D). This could be caused by overexpression or the tagging of the protein. Importantly, Cab45 deficient cells show the aberrant clustering of lysosomes in the perinuclear region (Figure S3D). Next, we tested PSAP-mCherry trafficking after biotin addition in the presence of late endocytic small GTPase Rab7-GFP. Our data revealed a decreased colocalization of PSAP with late endosomes in Cab45KO compared to HeLa wt cells (Figure S2D), indicating a role of Cab45 for correct localization of PSAP-mCherry to endolysosomal structures.

Connections between the change in lysosomal positioning and lysosomal function have been implied and investigated in the past (Trivedi et al., 2020; Bajaj et al., 2019). Therefore, we next asked if the aberrant lysosomal position in Cab45 deficient cells impacts the degradative activity of these lysosomes. To this end, we applied an assay to measure the bulk degradative activity of lysosomes. We loaded control and Cab45KO cells with DQ-BSA, a fluorogenic substrate for proteases quenched without protease activity. After endocytosis, DQ-BSA reaches the lysosomes, and the cleavage of DQ-BSA can measure their degradative activity by lysosomal proteases into fluorescent peptide fragments (Marwaha and Sharma et al.,.2017, Figure S3A). We analyzed the fluorescent signals in populations controlling Cab45 deficient cells by FACS. Endocytosis and trafficking of Atto-488 to lysosomes were used as a control for endocytosis and lysosomal trafficking from the plasma membrane. Both processes were intact in control compared to Cab45KO cells (Figure S 3B). Our results showed bright fluorescent DQ-BSA signals in control and Cab45KO cells, which were not present when cells were incubated with Bafilomycin A1, an inhibitor of lysosome acidification (Figure S3A). The analysis of broad populations cells by FACS showed no global change in the degradative activity of Cab45-deficient lysosomes (Figure S3A–S3C). These data suggested that Cab45 depletion has no impact on the bulk degradative activity of lysosomes. As DQ-BSA is a very unspecific substrate, changes in PRGN or PSAP would not be reflected in this assay. Furthermore, the question of how PRGN and PSAP impact the activity of other proteases is still under debate (Simon et al., 2022). For instance, GRN (derived from PGRN) peptides stimulate Cathepsin D (CatD) activity in cell-free assays. However, several reports have shown that depending on the cell type; these peptides also inhibit cathepsin D activity (Ward et al., 2017; Valdez et al., 2017; Götzl et al., 2018).

Nevertheless, we anticipate that the specific activities of PSAP and PGRN need to be analyzed in control and Cab45KO cells.

In conclusion, we show that Cab45 is critical for the lysosomal transport of PSAP and PRGN and positioning. This is exemplified by our results showing that in the absence of Cab45, the precursor forms of PSAP and PGRN are not efficiently captured in the TGN and are misrouted to the cell surface. We used HeLa cells as an experimental system for our approaches. We anticipate that the phenotypes observed here would be physiologically highly relevant in specialized cell types such as neurons (Rhinn et al., 2022). PSAP and PGRN trafficking in neurons is of high medical relevance as they emerge as significant players in neurodegenerative diseases (Tayebi et al., 2020; Paushter et al., 2018). PSAP is a central component in α-synuclein degradation (Mazzulli et al., 2016). Accumulation of α-synuclein in aging neurons induces synucleinopathies such as Parkinson's disease and dementia (Tayebi et al., 2020). PGRN is associated with frontotemporal lobar degeneration (FTLD), a form of early-onset dementia where TDP-43 proteinopathies cause the formation of ubiquitinated TDP-43-positive inclusion bodies (Evers et al., 2017; Neumann et al., 2007; Zhou et al., 2017 (2)). We have clearly defined Cab45 as a significant regulator of PSAP and PGRN trafficking to the lysosome. The mechanism, however, is not yet precise.

Nevertheless, based on the literature and our experiments that Cab45 influences either the segregation of cargo receptors in the TGN membrane or the recognition of lysosomal proteins and their receptors. We hypothesize that mistrafficking of these hydrolases and possibly other lysosomal proteins significantly impact lysosome positioning. Future work is required to test this hypothesis and investigate how Cab45 affects receptor-cargo binding. Our work has provided insights into the necessary components for lysosome biology under physiological and pathophysiological conditions.

Materials and Methods

Antisera

Antibodies used for the study are listed as follows: monoclonal antibodies (mABs) mouse β-actin (sigma, A-5441), mAB mouse prosaposin (Abnova, H0005660-M03), mAB mouse progranulin (invitrogen, MA1-187), mAB mouse cathepsin D (BD transduction Laboratories, 610801), polyclonal rabbit Sortilin/NT3 (abcam, ab16640), recombinant rabbit M6PR (cation independent) (abcam, ab124767), mAB rabbit LAMP1 (clone D2D11, 9091S, cell signaling), polyclonal antibody (pAB) sheep TGN46 (AHP500G, Bio-Rad), pAB rabbit Giantin (abcam, ab93281), mAB mouse Giantin (abcam, ab37266). The Cab45 antibody was generated in rabbits, as published by Crevenna et al., 2016. All primary antibodies for immunoblotting were diluted in 5% Bovine Serum Albumin (BSA, sigma) in TBS (1: 2 000). For application in immunostaining, primary antibodies were used in 1:500 dilution (1:1 000 for Giantin and TGN46) in 4% BSA (in PBS) or 0.1% Saponin in 3% BSA (in PBS), respectively.

Secondary antibodies for immunoblotting goat anti-mouse poly HRP (32230) and goat anti-rabbit poly HRP (32260) were purchased from ThermoScientific and used in 1:15 000 dilutions in 5% BSA in TBS.

Secondary antibodies for immunostaining Alexa Fluor donkey sheep488 (IgG H+L) (A11015), Alexa Fluor donkey mouse488 (IgG H+L) (A21202), Alexa Fluor donkey mouse594 (IgG H+L) (A21203), Alexa Fluor donkey rabbit488 (IgG H+L) (A21206), Alexa Fluor donkey rabbit 594 (IgG H+L) (A11037) were purchased from ThermoScientific and used in 1: 500 dilution in 4% BSA in PBS.

Cell Culture and cell lines

Cell lines were cultured in Dulbecco's Modified Eagle Medium (DMEM, Gibco) with 10% fetal bovine serum (FBS, Gibco) at 37°C and 5% CO2. Passaging was performed with 0.05% Trypsin-EDTA every 2-3 days to maintain single-layer growth.

The stable cell line Cab45-HA-wt (Cab45wt rescue) was generated by retrovirus transfection (Pfeifer et al., 2000) in Cab45KO background cells, as published previously (Crevenna et al., 2016). The Cab45KO cell line was generated using CRISPR (Crevenna et al., 2016).

SORT1KO, IGF2RKO, Sort1/IGF2R double KO cell lines, and parental HeLa were a gift from S. Ferguson (Yale School of Medicine, New Haven, CT, USA).

DNA manipulation and plasmid engineering

RUSH constructs were cloned using Gibson assembly. pIRESneo3_Str-LyzC-KDEL-SBP-EGFP was published previously (Deng et al., 2018).

Str-KDEL-Prosaposin-SBP-mCherry (Devireddy and Ferguson, 2021) was a gift from S. Ferguson (Yale School of Medicine, New Haven, CT, USA). BFP-GalT1 was received from C. Burd (Yale School of Medicine, New Haven, CT, USA) and gifted from J. Rothman (Yale School of Medicine, New Haven, CT, USA).

siRNA silencing

AllStars negative control (20 nM, Qiagen) was used as a negative control in all silencing experiments.

Cab45 siRNA was purchased from Invitrogen as an oligo:

5'-GGTCACGTGTCTTGGGACGAGTATA-3' (Cab45 Oligo 2) and used in several publications before (von Blume et al., 2012; Deng et al., 2018)

For general siRNA transfection, 20 nM siRNA and 8 μL HiPerfect transfection reagent (Qiagen) were mixed in 100 μL Opti-MEM™I reduced serum medium (Gibco by Life Technologies) and added to 6-well-plates containing cells in growth media.

For Cab45 silencing in secretion assays using 15 cm dishes, 800 uL Opti-MEM containing 70 μL HiPerfect + 7 μL siRNA were added to cells grown to 60% confluency. Further experiments were performed after 24h of siRNA transfection.

Transfection with DNA plasmids

Transient transfection with engineered plasmids described above was performed using 12 μL PEI (1.25 mg/mL, Alfa Aesar) and 1.5 μg DNA for immunofluorescence experiments. The reagent was incubated in 200 μL Opti-MEM reduced serum medium with 1.5 μg DNA for 15 min before adding to the cells cultured in 6-well-dishes (at least 60% confluent).

For Live Cell imaging, cells (70-80 % confluent) were cultured in 3.5 mm glass bottom dishes and transfected using Lipofectamine®2000 transfection reagent (Invitrogen). The mixtures containing each 150 μl Opti-MEM reduced serum medium with 3 μL Lipofectamine or DNA (150 ng BFP-GalTl and μg RUSH-construct) were incubated at room temperature for 5 min, then combined and incubated for 20 min. The solution was added to 1200 μL growth media on cells. After five h, the supernatant was exchanged for new growth media with Avidin (1 mg/mL).

hiSPECS analysis

Secretome analysis was performed using the high-performance secretome protein enrichment with click sugars (hiSPECS) method as described in detail by Tüshaus et al.,2020. In brief, cells were cultured in cultivation media in the presence of 50 μM ManNAz (ThermoFisher, 88904) for 48h, condition media was collected and filtered to clear it from cellular debris. Glycoprotein enrichment was conducted with Concanavalin A (Sigma, C7555) beads before performing the click reaction of azide-modified glycoproteins to DBCO-beads (Jena Bioscience CLK-1037) overnight at 4°C. After washing the proteins with SDS, UREA, and acetonitrile, they were digested with trypsin (on-bead). Desalted peptides were separated on an EASY-nLC 1200 UHPLC system (Thermo Fisher Scientific) using a 120 min gradient on a 30 cm long C18 column (self-packed, 75 μm ReproSil-Pur 120 C18- AQ resin Dr. Maisch GmbH). A Q-Exactive™ HF A Hybrid Quadrupole-Orbitrap™ mass spectrometer (Thermo Fisher Scientific) was used for this study. Data analysis was performed with MaxQuant software using standard settings besides a minimal peptide length of 6 (1% FDR on protein and peptide level).

Detection of proteins by immunostaining and immunoblotting

Cells were washed with PBS three times to detect proteins from cell lysate, then incubated with lysis buffer (1% Triton-X-100 in PBS) on ice. Secreted proteins were collected by cell culture supernatant concentration with Amicon®Ultra (20 mL, Millipore, Ultracel® - 10K) centrifugal filters. Proteins were separated by size using SDS-PAGE and 10% Acrylamide gels for further analysis.

For immunostaining, cells were grown on glass slides (#1.5, 12 mm diameter, EMS in 6-well dishes) to 60-70% confluency before transfection (see above). 24h after transfection, immunostaining was performed by fixing cells for 10 min with 4% fresh paraformaldehyde (PFA) (Electron Microscopy Sciences) in Dulbecco's Phosphate Buffered Saline (Gibco), then permeabilized with 0.2%Triton-X-100 and 0.5% SDS in 4% BSA solution for 3 min. Cells were washed three times with DPBS after each step. Unspecific binding was blocked by one h incubation with 4% BSA solution at room temperature or two h at 4C. Subsequently, cells were incubated with primary antibody overnight at four °C, after

washing with secondary antibody for one h at room temperature (RT). The glass slides were mounted using ProLong Gold antifade reagent with DAPI (Invitrogen) and imaged in confocal microscopy.

Immunostaining with LAMP1-antibody was changed according to the sensitivity of the antibody. Cells were grown as described above, then fixed with fresh 8% PFA in a 1:1 solution of DMEM and DPBS for 30 minutes at room temperature. Glass slides with the fixed cells were washed twice with DPBS. Permeabilization was performed with 0.1% saponin (ChemCruz) in DPBS for 15 minutes, followed by blocking with 3% BSA in DPS containing 0.1% saponin (20 min, RT). Primary and secondary antibodies were diluted in the blocking solution overnight (primary) and during 20-minute incubation (secondary). Glass slides were mounted as described above.

For immunoblotting, SDS gels were transferred to nitrocellulose membranes (0.2 μm, Bio-Rad) by the wet-blot system (Bio-Rad) in transfer buffer (25 mM Tris, 192 mM glycine, pH 8.3) containing 20% methanol at 105 V for 70 min. The membranes were blocked using 5% BSA in TBS for one h, RT, before incubation with primary antibody (4C, overnight) and secondary antibody (1h, RT). Membranes were washed with TBS + 0.1% Tween-20 three times (each 10 min) after primary and secondary antibody incubation. Antibodies were diluted in 5% BSA in TBS as described above and detected using chemiluminescence (Pierce™ ECL Western Blotting solution) on a ChemiDoc™ Touch Imaging system (Bio-Rad) imaging system.

Analysis of LAMP1 localization

For analysis of confocal images with LAMP1 immunostaining, ImageJ software was applied. The channels containing the LAMP1 fluorescent signal and the second channel in overexposure to visualize the outline of the whole cell were opened as separate images. The area of the LAMP1 signal and the entire cell were manually selected and determined as regions of interest (ROIs), then measured with the function ‘Measure’ in the ROI manager. ROI (LAMP1) was divided by ROI (whole cell) for quantification. The percentage ratio was plotted with GraphPad Prism9 and statistically analyzed using multiple nonparametric comparisons (Kruskal-Wallis test).

RUSH assay for fixed cell imaging

RUSH assays were performed as described in previous publications on fixed cells. Live cell imaging in combination with RUSH is described in detail as a trans-Golgi-exit assay. For RUSH assays with subsequent imaging of fixed cells, cells were grown on glass slides in 6-well-dishes. Transfection was done as described above, and the RUSH assay was performed 24h after transfection. To start the experiment, cells were washed once in PBS before adding DMEM containing 40 μM D-biotin (Fisher BioReagents) for different time points (20. 40, and 60 min). For 0 min control, no D-biotin was added. Cells were washed once with PBS before fixing with 4% paraformaldehyde in DPBS for 10 min. After three times washing with PBS, cells on glass slides were mounted with ProLong Gold antifade with DAPI, and images were acquired using a confocal laser-scanning microscope (Carl

Zeiss; LSM 880; 63x NA1.4 Plan-Apochromat oil objective) with ZEN 2010 software in z-stacks (0.35 μM slices thickness).

Quantifying the number of post-Golgi vesicles was determined using the ImageJ macro Count_Fixed_Vesicles_V1.3 (published on GitHub by M. Pakdel. 2019). The macro uses Fiji's *particle analyzer* function on generated binary images. Larger objects, like fragments of organelles, were omitted using a defined size of 4- 20 pixels for the recognized and counted things.

RUSH assay for live-cell imaging (trans-Golgi exit assay)

For the live-cell-imaging experiment with RUSH, cells were seeded on 35 mm dishes with 20 mm diameter glass bottoms. Transfection was performed as described above. For the trans-Golgi exit assay, the culture media was exchanged with imaging media (DMEM without phenol-red + 10 % FBS). After setting up the imaging stage (Nikon eclipse Ti2, LWD NA=052m with stage top Piezo) and spinning disk confocal microscope (CSUXfw-06p-01, Yokogawa), including heating chamber to 37°C, the cells were imaged without D-biotin to determine the focal plane (locked with PFS) on a CFI Plan Apo Lambda 60x/NA 1.4 oil objective (Nikon). The RUSH assay started after washing the cells carefully with PBS and adding new imaging media containing 40 μM D-biotin and 100 μM cycloheximide (dot-scientific inc.). Images were acquired immediately in 5x6 fields of view with 10% tile stitching for two h every 5 min. A laser combiner with 405, 488, 561, and 640 nm (Agilent) was used for the respective fluorescence detection of mCherry or BFP. NIS element software was used to monitor imaging and save acquired images as stacked two-channel files.

Images were further processed with ImageJ and BioFormats add-ons. ImageJ threshold function (default setting) was used to transform image stacks of the trans-Golgi marker (BFP-GalT1) into binary files for applying the particle analyzer function. A size of 1-100 nM (including holes, excluding edges) was set to recognize objects that classify as Golgi elements in the BFP channel, which are then saved as regions of interest (ROI). ROIs were overlaid with the signal of the RUSH-construct and mean fluorescence intensity (F.I.) in this ROI measured. Data was saved and copied into Excel to refine and calculate the mean signal intensity for each time point and cell. Maximal and minimal F.I. for each cell of all time points were subtracted and normalized by dividing by the highest value (= 1) and lowest value (= 0). Cells with intact and compact trans-Golgi marker staining throughout the measurement were considered for analysis. For plotting the trans-Golgi exit, the peak of F.I. in the trans-Golgi marker ROI was set as t=0. All mean F.I. from that time point till the end of the measurement were plotted. The half-life of the RUSH construct in the trans-Golgi marker ROI was determined by applying non-linear regression with an exponential function. GraphPad Prism 9 built-in curve fit program was used for analysis with exponential one-phase decay function.

Secretion assays

Cells were cultured in 15 cm tissue culture dishes and transfected with siRNA as described above. After 24h, the media was exchanged to fresh culture media to recover cells before

starting starvation when the cells were at least 75% confluent. Starvation was performed after three times washing in DPBS and changing to DMEM without FBS containing protease inhibitor (cOmplete mini protease inhibitor tablets, Roche). The cell culture supernatant was collected after 24h, filtered with 25mm 0.45 μM Acrodisc(R) filters (Pall Corporation), and concentrated to approximately 500 uL by using Amicon®Ultra (20 mL, Millipore, Ultracel® - 10K, catalog: UFC901096) at four °C, 4347xg, 50 minutes. Volumes were equalized with DPBS, and samples were prepared according to protein levels of cell lysate.

Intracellular proteins in cell lysates were received after incubation with 500 μL lysis buffer (1x PBS + 1% Triton-X-100) for 20 min on ice. Cell debris was removed by centrifugation (20 min, four °C, 21100 x g). Cleared lysate of each sample was equalized with lysis buffer to the same volume before measuring the relative protein concentration with Bradford (Bio-Rad) on Nanodrop ONE(c) (ThermoScientific).

The samples were denatured with 4x Laemmli buffer + 4% β-mercaptoethanol (95°C, 3 min) and separated by size using SDS-PAGE in 10% Acrylamide-SDS gels. Another protein detection was achieved with immunoblotting.

Secretion assay and pulldown

Agarose beads (Protein A/G PLUS-Agarose, sc-2003, Santa Cruz Biotechnology Inc.) were washed 3 times with 1 mL DPBS per sample, then blocked by incubation with 1% BSA in PBS for 30 min to 1h at 4°C on a rotation wheel. The beads were washed 3 times with 1 mL DPBS (3400 rpm, 4 °C) and incubated with PSAP-antibody (4 μL per 35 μL of bead slurry) overnight (4 °C, rotation wheel). The antibody-bound beads were washed 3 times with 1 mL DPBS and once with IP buffer (50 mM TRIS, 100 mM NaCl, 0.1 % Triton-X-100, pH 7.4) containing new cOmplete protease inhibitor tablet (Roche), then stored on ice before usage.

HeLa and Cab45KO cells were seeded into 10 cm tissue culture dishes as described for secretion assays above to apply the secretion assay at short periods for pulldown experiments. At 85 - 95 % confluency, the assay was started by adding 3.5 mL of fresh growth media to the cells for 2 h or 4h. The growth medium was collected, filtered and cells were harvested as described above and lysed in 350 μL IP lysis buffer for 20 min on ice. The lysate was separated by using a needle (27G) for 10 times, then cleared from cell debris by centrifugation (13000 rpm, 20 min, 4°C). Protein concentrations were determined using Bradford after equalizing to the same volume. Supernatants were equalized to the same volume between HeLa and Cab45KO cells and then diluted according to the cell lysates to a maximal volume of 2.8 mL Inputs (50 μL) and stored for SDS gel electrophoresis at 4°C. Supernatants were divided into two 1.5-mL tubes with each 20 μL (beads slurry) of prepared, washed antibody-bound agarose beads. The samples were incubated (overnight, 4 °C, rotation wheel), then washed three times with IP-buffer (with protease inhibitor, 3400 rpm, 3 min, 4 °C). With the final washing step, the supernatant was obliterated carefully. Proteins bound to PSAP-antibody on the beads were eluted by boiling in 2x Laemmli buffer (95°C, 10 min) and collected as an IP sample. Subsequently, the proteins in the IP sample and Input were analyzed via western blotting using an anti-PSAP antibody (Abnova, H0005660-M03, 1: 2 000, 5% BSA in TBS).

cDNA preparation for qRT-PCR

Total RNA was extracted from cells using RNeasy Mini Kit (Qiagen) according to the manufacturer's instructions. Concentrations were measured using Nanodrop® and used for cDNA preparation with RevertAid RT Reverse Transcription Kit (ThermoFisher Scientific) following the manufacturer's protocol.

The cDNA was stored at −80°C for further usage in qRT-PCR experiments.

qRT-PCR

Primer design was based on genome browser results for the gene of interest mRNA. The sequence was copied into PerlPrimer software to receive the following primer sequences:

SDF4 1F: 5'-CGCTGGATCATGGAGAAGAC-3'

SDF4 1R: 5'-GACTTCCTGTGTTTCCTCATCC-3'

PSAP 1F: 5'-AGAGCTGGACATGACTGAGG-3'

PSAP 1R: 5'-GTTCTTGCATATGTCGGCCA-3'

GRN 1F: 5'-CTTCTGGACAAATGGCCCAC-3'

GRN 1R: 5'-GGAGTTGTTACCTGATCTTTGGA-3'

All RT-PCR experiments were performed using 5 μL SYBR(R) green qPCR Readymix™ iQ (KiCqStart™, sigma), 4 ʊL cDNA (5 nM), 0.6 ʊL (sense and antisense) primers (10 nM) and 0.4 μL DNase free water in duplicates. For preparing the calibration curves, diluted cDNA from control, siCab45, and non-treated Hela were mixed equally in serial dilutions. Amplification with the respective primers was performed and recorded with CFX96, and data were further analyzed with CFX manager software version 3.0 (Bio-Rad).

Lysosomal activity assay with DQ-BSA

HeLa wt and Cab45KO cells were plated in 6 well plates at the density 10^5 per well in DMEM complete grown medium. The next day, the media was removed, and dishes were washed with 2 ml of DPBS. DQ™ Green BSA (Invitrogen; D12050) was added in prewarmed Trafficking media (Marwaha et al., 2017) to a final 10 μg/mL concentration. Similar procedures were performed for negative control samples before treatment with the addition of 100 nM Bafilomycin A. Cells were incubated at 37 °C (5% CO_2, humified) for 1 h and 6 h, respectively. At 1 h and 6 h time points, cells were fixed with 4% PFA in DPBS and collected for FACS analysis. FACS analysis was performed on a BD LSRII machine using the green channel. Untreated cells were used as a reference.

A similar procedure with subsequent FACS analysis was performed using BSA-GFP to confirm that endocytosis rates were not affected. For IF imaging, cells were grown on German Glass Coverslips (EMS;#72290-04) and proceeded as described above for immunofluorescence analysis.

Surface biotinylation

To check the expression of the receptor proteins IGF2R and SORT1 on the cell surface of HeLa and. Cab45KO cells, pulldown of biotinylated cell surface proteins NeutrAvidin agarose beads (Pierce, 20353) was performed. Cells were seeded in 10 cm culture dishes (150 000 cells per dish) until 70-80% confluent. After 18 – 24 h, cells were washed (2 times, 4 mL) with ice-cold DPBS (1x) on ice. Cells from each cell line were labeled with Sulfo-NHS-SS-biotin (250 μg/mL, 2.5 mL per dish) for 90 min at 4°C (rocking platform). Excess biotin was removed by washing once with ice-cold glycine in DPBS (150 mM) before quenching the biotinylation reaction with incubation in the same glycine solution for 25 min (5 mL/ dish rocking platform). Cells were washed with ice-cold DPBS, subsequently collected with cell scrapers, and lysed in 1 ml Lysis buffer (100 mM Tris-HCL, 150 mM NaCl, 0.1 % SDS, 1% Triton, 1% deoxycholic acid, pH 7.4, and protease inhibitor tablets (Roche) for 30 min on ice. Cell lysates were separated from cell debris by centrifugation for 15 min at 14000 rpm (4°C). NeutrAvidin beads were prepared for incubation by washing with 0.5 mL DPBS twice and 0.5 mL Lysis buffer twice (3400 rpm, 4°C, 3 min). After analysis of total protein content in each sample by Bradford (absorption λ = 595 nm), equal amounts of cell lysates were incubated with 150 μl NeutrAvidin bead slurry overnight at 4°C (rotating wheel). Subsequently, the beads were washed with lysis buffer (1 mL, 5 times) on ice and centrifuged (3400 rpm, 4 min). Then, biotinylated proteins were eluted with 80 μl Laemmli sample buffer containing 50 mM DTT (10 min, 95°C) and analyzed by SDS-PAGE and western blotting with antibodies recognizing IGF2R (Abcam, ab124767, ERP6599, 1: 2 000, 5% BSA in TBS) and SORT1 (Abeam, ab 16640, GR3379711, 1: 2 000, 5% BSA in TBS), β-integrin (BD Transduction Laboratories TMClone 18/CD29, 1 : 1 000, 5% milk in TBS).

Statistical Analysis

All statistical analyses were performed with samples from at least three independent experiments by using GraphPad Prism 9. For statistical analysis using t-tests, numeric data between the control and a treated sample were compared as unpaired t-tests of two groups using a parametric test (assume Gaussian distribution). For statistical analysis of densiometric blots of secretion assays (Fig. 2B, D; 3C, E, G; S1), a comparison of Pearson's coefficient (Fig. 5D) and Half-life values (Fig. 4E), we assumed that both populations have the same standard deviation. We used a confidence interval of 95% unless the spread of the numerical values of the analyzed populations were bigger, i.e., when the population's average is not identical to the peak of a Gaussian distribution.

For statistical analysis of numbers (ratio) of objects in a particular area (Fig. 5B), the Kruskal-Wallis test was used as an unpaired test of groups, not assuming a Gaussian distribution (non-parametric test) to compare the medians of the compared populations.

Supplementary Material

Refer to Web version on PubMed Central for supplementary material.

Acknowledgments

We thank Christopher Burd, Anup Parchure, and Jan Parolek for constructive discussions. Julia von Blume is funded by a Yale-start grant and by the National Institute of General Medical Sciences of the United States National Institutes of Health under the award number GM134083-01, an Administrative Supplement 3R01GM134083-03S1, and a Project and Feasibility award from Yale Diabetic Research Center (GR112420). Shawn Ferguson is funded by Bluefield Project to Cure FTD (SD and SMF), The Parkinson's Disease Foundation (SMF), and the NIH (AG062210) to SMF. Stefan Lichtenthaler is funded by the Deutsche Forschungsgemeinschaft (DFG, German Research Foundation) under Germany's Excellence Strategy within the Munich Cluster for Systems framework Neurology (EXC 2145 SyNergy– ID 390857198).

References

Bajaj L, Lotfi P, Pal R, Ronza AD, Sharma J, and Sardiello M. 2019. Lysosome biogenesis in health and disease. J Neurochem. 148:573–589. [PubMed: 30092616]

Boncompain G, and Perez F. 2012. Synchronizing protein transport in the secretory pathway. Curr Protoc Cell Biol. Chapter 15:Unit 15 19.

Bonifacino JS, and Neefjes J. 2017. Moving and positioning the endolysosomal system. Curr Opin Cell Biol. 47:1–8. [PubMed: 28231489]

Braulke T, and Bonifacino JS. 2009. Sorting of lysosomal proteins. Biochim. Biophys. Acta 1793:605–614. 10.1016/j.bbamcr.2008.10.016) [PubMed: 19046998]

Cheng XT, Xie YX, Zhou B, Huang N, Farfel-Becker T, and Sheng ZH. 2018. Characterization of LAMP1-labeled nondegradative lysosomal and endocytic compartments in neurons. J Cell Biol. 217:3127–3139. [PubMed: 29695488]

Coutinho MF, Prata MJ, and Alves S. 2012. A shortcut to the lysosome: the mannose-6-phosphate-independent pathway. Mol Genet Metab. 107:257–266. [PubMed: 22884962]

Crevenna AH, Blank B, Maiser A, Emin D, Prescher J, Beck G, Kienzle C, Bartnik K, Habermann B, Pakdel M, Leonhardt H, Lamb DC, and von Blume J. 2016. Secretory cargo sorting by Ca2+-dependent Cab45 oligomerization at the trans-Golgi network. J Cell Biol. 213:305–314. [PubMed: 27138253]

Curwin AJ, von Blume J, and Malhotra V. 2012. Cofilin-mediated sorting and export of specific cargo from the Golgi apparatus in yeast. Mol Biol Cell. 23:2327–2338. [PubMed: 22553351]

Deng Y, Pakdel M, Blank B, Sundberg EL, Burd CG, and von Blume J. 2018. Activity of the SPCA1 Calcium Pump Couples Sphingomyelin Synthesis to Sorting of Secretory Proteins in the Trans-Golgi Network. Dev Cell. 47:464–478 e468. [PubMed: 30393074]

Devireddy S, and Ferguson SM. 2022. Efficient progranulin exit from the ER requires its interaction with prosaposin, a Surf4 cargo. J Cell Biol. 221(2), e202104044. [PubMed: 34919127]

Di Martino R, Sticco L, and Luini A. 2019. Regulation of cargo export and sorting at the trans-Golgi network. FEBSLett. 593:2306–2318.

Doray B, Ghosh P, Griffith J, Geuze HJ, and Kornfeld S. 2002. Cooperation of GGAs and AP-1 in packaging MPRs at the trans-Golgi network. Science. 297:1700–1703. [PubMed: 12215646]

Dunphy WG, and Rothman JE. 1985. Compartmental organization of the Golgi stack. Cell. 42:13–21. [PubMed: 3926324]

Evers BM, Rodriguez-Navas C, Tesla RJ, Prange-Kiel J, Wasser CR, Yoo KS, McDonald J, Cenik B, Ravenscroft TA, Plattner F, Rademakers R, Yu G, White CL 3rd, and Herz J. 2017. Lipidomic and Transcriptomic Basis of Lysosomal Dysfunction in Progranulin Deficiency. Cell Rep. 20:2565–2574. [PubMed: 28903038]

Ghosh P, Dahms NM, and Kornfeld S. 2003. Mannose 6-phosphate receptors: new twists in the tale. Nat Rev Mol Cell Biol. 4:202–212. [PubMed: 12612639]

Glick BS, Elston T, and Oster G. 1997. A cisternal maturation mechanism can explain the asymmetry of the Golgi stack. FEBS Lett. 414:177–181. [PubMed: 9315681]

Glick BS, and Luini A. 2011. Models for Golgi traffic: a critical assessment. Cold Spring Harb Perspect Biol. 3:a005215. [PubMed: 21875986]

Gopalakrishnan MM, Grosch HW, Locatelli-Hoops S, Werth N, Smolenova E, Nettersheim M, Sandhoff K, and Hasilik A. 2004. Purified recombinant human prosaposin forms oligomers that bind procathepsin D and affect its autoactivation. Biochem J. 383:507–515. [PubMed: 15255780]

Götzl JK, Colombo AV, Fellerer K, Reifschneider A, Werner G, Tahirovic S, Haass C, and Capell A. 2018. Early lysosomal maturation deficits in microglia triggers enhanced lysosomal activity in other brain cells of progranulin knockout mice. Mol Neurodegener. 13(1):48. doi: 10.1186/s13024-018-0281-5. [PubMed: 30180904]

Hasilik A, Wrocklage C, and Schroder B. 2009. Intracellular trafficking of lysosomal proteins and lysosomes. Int J Clin Pharmacol Ther. 47 Suppl 1:S18–33. [PubMed: 20040308]

Hassan AJ, Zeng J, Ni X, and Morales CR. 2004. The trafficking of prosaposin (SGP-1) and GM2AP to the lysosomes of TM4 Sertoli cells is mediated by sortilin and monomeric adaptor proteins. Mol Reprod Dev. 68:476–483. [PubMed: 15236333]

Hecht TK, Blank B, Steger M, Lopez V, Beck G, Ramazanov B, Mann M, Tagliabracci V, and von Blume J. 2020. Fam20C regulates protein secretion by Cab45 phosphorylation. J Cell Biol. 219:6.

Hiesberger T, Huttler S, Rohlmann A, Schneider W, Sandhoff K, and Herz J. 1998. Cellular uptake of saposin (SAP) precursor and lysosomal delivery by the low density lipoprotein receptor-related protein (LRP). EMBO J. 17:4617–4625. [PubMed: 9707421]

Kim MJ, Jeong H, and Krainc D. 2022. Lysosomal ceramides regulate cathepsin B-mediated processing of saposin C and glucocerebrosidase activity. Hum Mol Genet. 31(14):2424–2437. doi: 10.1093/hmg/ddac047. [PubMed: 35181782]

Klumperman J, Hille A, Veenendaal T, Oorschot V, Stoorvogel W, von Figura K, and Geuze HJ. 1993. Differences in the endosomal distributions of the two mannose 6-phosphate receptors. J Cell Biol. 121:997–1010. [PubMed: 8099077]

Kuhn PH, Koroniak K, Hogl S, Colombo A, Zeitschel U, Willem M, Volbracht C, Schepers U, Imhof A, Hoffmeister A, Haass C, Rossner S, Brase S, and Lichtenthaler SF. 2012. Secretome protein enrichment identifies physiological BACE1 protease substrates in neurons. EMBO J. 31:3157–3168. [PubMed: 22728825]

Laurent-Matha V, Lucas A, Huttler S, Sandhoff K, Garcia M, and Rochefort H. 2002. Procathepsin D interacts with prosaposin in cancer cells but its internalization is not mediated by LDL receptor-related protein. Exp Cell Res. 277:210–219. [PubMed: 12083803]

Lefrancois S, Zeng J, Hassan AJ, Canuel M, and Morales CR. 2003. The lysosomal trafficking of sphingolipid activator proteins (SAPs) is mediated by sortilin. EMBO J. 22:6430–6437. [PubMed: 14657016]

Lingappa VR, and Blobel G. 1980. Early events in the biosynthesis of secretory and membrane proteins: the signal hypothesis. Recent Prog Horm Res. 36:451–475. [PubMed: 6997945]

Marwaha R, and Sharma M. 2017. DQ-Red BSA Trafficking Assay in Cultured Cells to Assess Cargo Delivery to Lysosomes. Bio Protoc. 7(19):e2571.

Mazzulli JR, Zunke F, Isacson O, Studer L, and Krainc D. 2016. Alpha-synuclein-induced lysosomal dysfunction occurs through disruptions in protein trafficking in human midbrain synucleinopathy models. Proc. Natl. Acad. Sci. U. S. A 113, 1931–1936. [PubMed: 26839413]

Miller EA and Barlowe C. 2010. Regulation of coat assembly--sorting things out at the ER. Curr Opin Cell Biol. 22: 447–453. [PubMed: 20439155]

Mostov KE, and Cardone MH. 1995. Regulation of protein traffic in polarized epithelial cells. Bioessays. 17:129–138. [PubMed: 7748163]

Neumann M, Kwong LK, Sampathu DM, Trojanowski JQ, and Lee VM. 2007. TDP-43 proteinopathy in frontotemporal lobar degeneration and amyotrophic lateral sclerosis: protein misfolding diseases without amyloidosis. Arch Neurol. 64:1388–1394. [PubMed: 17923623]

Ni X, Canuel M, and Morales CR. 2006. The sorting and trafficking of lysosomal proteins. Histol Histopathol. 21:899–913. [PubMed: 16691542]

O'Brien JS and Kishimoto Y. 1991. Saposin proteins: Structure, function, and role in human lysosomal storage disorders. FASEB J. 5:301–308. [PubMed: 2001789]

Okreglak V, and Drubin DG. 2007. Cofilin recruitment and function during actin-mediated endocytosis dictated by actin nucleotide state. J Cell Biol. 178:1251–1264. [PubMed: 17875745]

Paushter DH, Du H, Feng T, and Hu F. 2018. The lysosomal function of progranulin, a guardian against neurodegeneration. Acta Neuropathol. 6(1):1–17. doi: 10.1007/s00401-018-1861-8.

Pérez-Victoria FJ, Mardones GA, and Bonifacino JS. 2008. Requirement of the human GARP complex for mannose 6-phosphate-receptor-dependent sorting of cathepsin D to lysosomes. Mol Biol Cell. 19(6):2350–62. doi: 10.1091/mbc.e07-11-1189. [PubMed: 18367545]

Pohlmann R, Boeker MW, and von Figura K. 1995. The two mannose 6-phosphate receptors transport distinct complements of lysosomal proteins. J Biol Chem. 270:27311–27318. [PubMed: 7592993]

Pu J, Guardia CM, Keren-Kaplan T, and Bonifacino JS. 2016. Mechanisms and functions of lysosome positioning. J Cell Sci. 129:4329–4339. [PubMed: 27799357]

Puertollano R, Aguilar RC, Gorshkova I, Crouch RJ, and Bonifacino JS. 2001. Sorting of mannose 6-phosphate receptors mediated by the GGAs. Science. 292:1712–1716. [PubMed: 11387475]

Qian M, Sleat DE, Zheng H, Moore D, and Lobel P. 2008. Proteomics analysis of serum from mutant mice reveals lysosomal proteins selectively transported by each of the two mannose 6-phosphate receptors. Mol Cell Proteomics. 7:58–70. [PubMed: 17848585]

Quistgaard EM, Madsen P, Groftehauge MK, Nissen P, Petersen CM, and Thirup SS. 2009. Ligands bind to Sortilin in the tunnel of a ten-bladed beta-propeller domain. Nat Struct Mol Biol. 16:96–98. [PubMed: 19122660]

Ramazanov BR, Tran ML, and von Blume J. 2021. Sending out molecules from the TGN. Curr Opin Cell Biol. 71:55–62. [PubMed: 33706234]

Reitman ML, Varki A, and Kornfeld S. 1981. Fibroblasts from patients with I-cell disease and pseudo-Hurler polydystrophy are deficient in uridine 5'-diphosphate-N-acetylglucosamine: glycoprotein N-acetylglucosaminylphosphotransferase activity. J Clin Invest. 67:1574–1579. [PubMed: 6262380]

Rhinn H, Tatton N, McCaughey S, Kurnellas M, and Rosenthal A. 2022. Progranulin as a therapeutic target in neurodegenerative diseases. Trends Pharmacol Sci. 43(8):641–652. doi: 10.1016/j.tips.2021.11.015. [PubMed: 35039149]

Saftig P, and Klumperman J. 2009. Lysosome biogenesis and lysosomal membrane proteins: trafficking meets function. Nat Rev Mol Cell Biol. 10:623–635. [PubMed: 19672277]

Scherer PE, Lederkremer GZ, Williams S, Fogliano M, Baldini G, Lodish HF. 1996. Cab45, a novel (Ca2+)-binding protein localized to the Golgi lumen. J Cell Biol. 133 (2): 257–268. [PubMed: 8609160]

Simon MS, Logan T, DeVos SL, and Di Paolo G. 2022. Lysosomal functions of progranulin and implications for treatment of frontotemporal dementia. Trends Cell Biol. DOI: 10.1016/j.tcb.2022.09.006.

Sleat DE, Della Valle MC, Zheng H, Moore DF, and Lobel P. 2008. The mannose 6-phosphate glycoprotein proteome. J Proteome Res. 7:3010–3021. [PubMed: 18507433]

Stalder D, and Gershlick DC. 2020. Direct trafficking pathways from the Golgi apparatus to the plasma membrane. Semin Cell Dev Biol. 107:112–125. [PubMed: 32317144]

Staudt C, Puissant E, and Boonen M. 2016. Subcellular Trafficking of Mammalian Lysosomal Proteins: An Extended View. Int J Mol Sci. 18.

Tang BL 2001. Protein trafficking mechanisms associated with neurite outgrowth and polarized sorting in neurons. J Neurochem. 79:923–930. [PubMed: 11739603]

Tayebi N, Lopez G, Do J, and Sidransky E. 2020. Pro-cathepsin D, Prosaposin, and Progranulin: Lysosomal Networks in Parkinsonism. Trends Mol Med. 26:913–923. [PubMed: 32948448]

Trivedi PC, Bartlett JJ, and Pulinilkunnil T. 2020. Lysosomal Biology and Function: Modern View of Cellular Debris Bin. Cells. 9:1131. [PubMed: 32375321]

Tüshaus J, Muller SA, Kataka ES, Zaucha J, Sebastian Monasor L, Su M, Guner G, Jocher G, Tahirovic S, Frishman D, Simons M, and Lichtenthaler SF. 2020. An optimized quantitative proteomics method establishes the cell type-resolved mouse brain secretome. EMBO J. 39:e105693. [PubMed: 32954517]

Valdez C, Wong YC, Schwake M, Bu G, Wszolek ZK, and Krainc D. 2017. Progranulin-mediated deficiency of cathepsin D results in FTD and NCL-like phenotypes in neurons derived from FTD patients. Hum Mol Genet. 26(24):4861–4872. doi: 10.1093/hmg/ddx364. [PubMed: 29036611]

von Blume J, Alleaume AM, Cantero-Recasens G, Curwin A, Carreras-Sureda A, Zimmermann T, van Galen J, Wakana Y, Valverde MA, and Malhotra V. 2011. ADF/cofilin regulates secretory cargo sorting at the TGN via the Ca2+ ATPase SPCA1. Dev Cell. 20:652–662. [PubMed: 21571222]

von Blume J, Alleaume AM, Kienzle C, Carreras-Sureda A, Valverde M, and Malhotra V. 2012. Cab45 is required for Ca(2+)-dependent secretory cargo sorting at the trans-Golgi network. J Cell Biol. 199:1057–1066. [PubMed: 23266954]

von Blume J, Duran JM, Forlanelli E, Alleaume AM, Egorov M, Polishchuk R, Molina H, and Malhotra V. 2009. Actin remodeling by ADF/cofilin is required for cargo sorting at the trans-Golgi network. J Cell Biol. 187:1055–1069. [PubMed: 20026655]

von Blume J, and Hausser A. 2019. Lipid-dependent coupling of secretory cargo sorting and trafficking at the trans-Golgi network. FEBS Lett. 593:2412–2427. [PubMed: 31344259]

Wahe A, Kasmapour B, Schmaderer C, Liebl D, Sandhoff K, Nykjaer A, Griffiths G, and Gutierrez MG. 2010. Golgi-to-phagosome transport of acid sphingomyelinase and prosaposin is mediated by sortilin. J Cell Sci. 123:2502–2511. [PubMed: 20571055]

Ward ME, Chen R, Huang HY, Ludwig C, Telpoukhovskaia M, Taubes A, Boudin H, Minami SS, Reichert M, Albrecht P, Gelfand JM, Cruz-Herranz A, Cordano C, Alavi MV, Leslie S, Seeley WW, Miller BL, Bigio E, Mesulam MM, Bogyo MS, Mackenzie IR, Staropoli JF, Cotman SL, Huang EJ, Gan L, and Green AJ. 2017. Individuals with progranulin haploinsufficiency exhibit features of neuronal ceroid lipofuscinosis. Sci Transl Med. 9(385):eaah5642. doi: 10.1126/scitranslmed.aah5642. [PubMed: 28404863]

Yang C, and Wang X. 2021. Lysosome biogenesis: Regulation and functions. J Cell Biol. Jun 7;220(6):e202102001. doi: 10.1083/jcb.202102001. [PubMed: 33950241]

Zhang T, Du H, Santos MN, Wu X, Pagan MD, Trigiani LJ, Nishimura N, Reinheckel T, and Hu F. 2022. Differential regulation of progranulin derived granulin peptides. Mol Neurodegener. 17(1):15. doi: 10.1186/s13024-021-00513-9. [PubMed: 35120524]

Zhang Z, Yue P, Lu T, Wang Y, Wei Y, and Wei X. 2021. Role of lysosomes in physiological activities, diseases, and therapy. J Hematol Oncol. 14:79. [PubMed: 33990205]

Zheng Y, Brady OA, Meng PS, Mao Y, and Hu F. 2011. C-terminus of progranulin interacts with the beta-propeller region of sortilin to regulate progranulin trafficking. PLoS One. 6:e21023. [PubMed: 21698296]

Zhou X, Sullivan PM, Sun L, and Hu F. 2017. The interaction between progranulin and prosaposin is mediated by granulins and the linker region between saposin B and C. J Neurochem. 143:236–243. [PubMed: 28640985]

Zhou X, Sun L, Bracko O, Choi JW, Jia Y, Nana AL, Brady OA, Hernandez JCC, Nishimura N, Seeley WW, and Hu F. 2017. Impaired prosaposin lysosomal trafficking in frontotemporal lobar degeneration due to progranulin mutations. Nat Commun. 8:15277. [PubMed: 28541286]

Zhou X, Paushter DH, Feng T, Pardon CM, Mendoza CS, and Hu F. 2017. Regulation of cathepsin D activity by the FTLD protein progranulin. Acta Neuropathol. 134:151–153. [PubMed: 28493053]

Zhou X, Paushter DH, Feng T, Sun L, Reinheckel T, Hu F. 2017. Lysosomal processing of progranulin. Mol Neurodegener. 12:62. [PubMed: 28835281]

Zhou X, Sun L, Bracko O, Choi JW, Jia Y, Nana AL, Brady OA, Hernandez JCC, Nishimura N, Seeley WW, and Hu F. 2017. Impaired prosaposin lysosomal trafficking in frontotemporal lobar degeneration due to progranulin mutations. Nat Commun. 8:15277. [PubMed: 28541286]

Zhou X, Sun L, Bastos de Oliveira F, Qi X, Brown WJ, Smolka MB, Sun Y, and Hu F. 2015. Prosaposin facilitates sortilin-independent lysosomal trafficking of progranulin. J Cell Biol. 210:991–1002. [PubMed: 26370502]

Synopsis

Here we describe a novel role of Cab45 in lysosomal export from the TGN. Cells lacking Cab45 accumulate perinuclear lysosomes and hypersecrete a subset of lysosomal hydrolases including progranulin (PRGN) and prosaposin (PSAP).

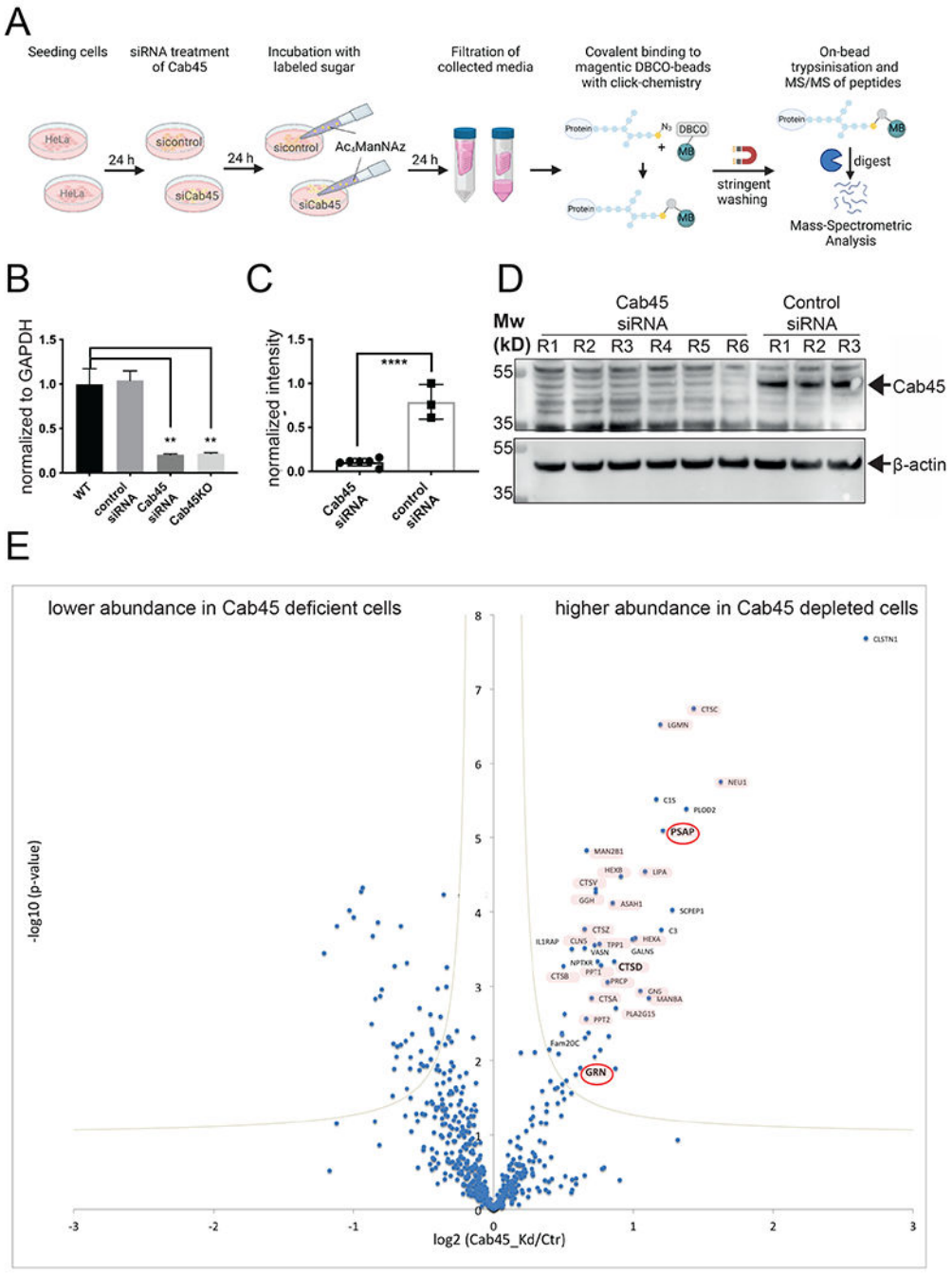

Figure 1. hiSPECS screening revealed that Cab45 deficient HeLa cells secrete high amounts of lysosomal hydrolases compared to control cells

(A). Schematic workflow of hiSPECS (Tüshaus et al., 2020) secretome analysis of control and Cab45 siRNA treated HeLa cells (created with biorender). N-azido-acetylated-mannosamine-tetraacylated (Ac4ManNAZ, labeling sugar) was added to the cell culture media of HeLa cells during siRNA treatment (24 h). The cell culture supernatant was prepared by filtration to remove cellular debris for subsequent click-chemistry to bind labeled glycoproteins to DBCO magnetic beads. Stringent washing was performed to

eliminate contaminations, and peptides were released from the beads by tryptic digest and analyzed via mass spectrometry. Control experiments to prove the efficiency of Cab45 silencing were performed with qRT-PCR **(B)** and immunoblotting with quantification of the normalized intensity of western blot bands by densitometry **(C, D)**. Cab45 mRNA expression in Cab45 siRNA-treated cells was reduced compared with that in wild-type (wt) and control cells. It was comparable in Cab45 knockout (KO) cells, whereas Cab45 protein levels quantified via western blotting were significantly decreased (****) compared with those in control **(C)**. **(E)** Volcano plot of hiSPECS results shows hits of for proteins with significantly or lower secretion in siCab45- versus control-treated cells (left and right side, respectively, with gene names) correlating p-value (−log10) vs. Cab45 knockdown (KD) / control (log2). Most (70%) of hypersecreted proteins upon KD of Cab45 are lysosomal hydrolases (pink shade). Examples of prosaposin (PSAP), and progranulin (GRN), are highlighted with a red circle.

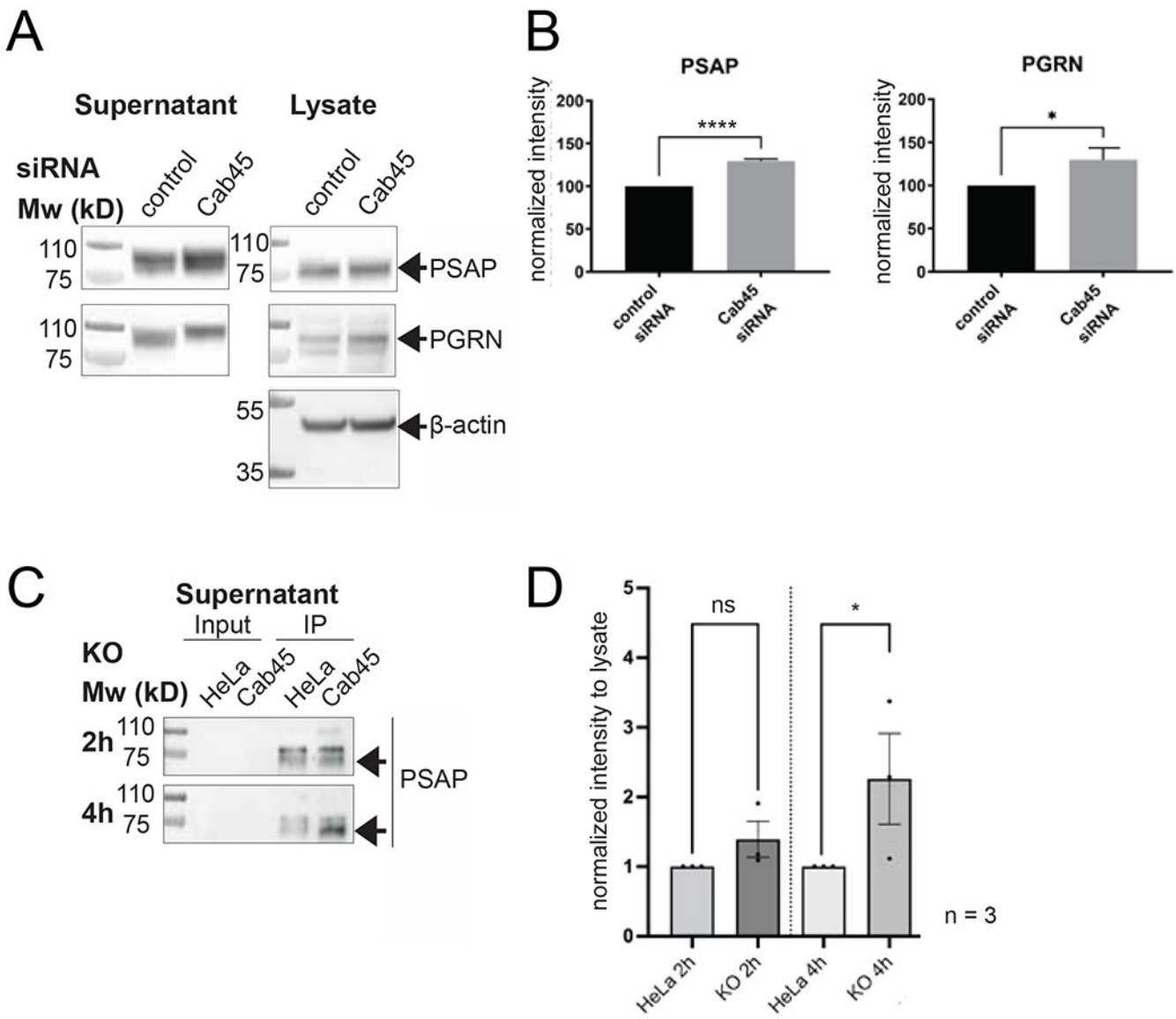

Figure 2. Validation of the hypersecretion phenotype in Cab45-deficient cells

(A) Representative immunoblot images of cell culture supernatants and lysates comparing protein levels of PSAP and PGRN in control and Cab45 siRNA treated HeLa wt cells. **(B)** Densiometric quantification of the western blot bands from three independent experiments in **A** shows a significantly higher secretion of PSAP (**** ($p<0.0001$); 1.3-fold higher) and PGRN (* ($p = 0.0206$); 1.3-fold higher) in Cab45 siRNA-treated cells. **Statistical analysis (t-test) includes three independent experiments; error bars depict SD. (C)** Representative immunoblots of HeLa wt compared to Cab45KO cell supernatants with subsequent pulldown on agarose beads incubated with PSAP-antibody. Secretion assays were performed for 2 and 4 h in serum-containing media; images show protein inputs and IPs. **(D)** Bar graphs show a consistent increase of PSAP levels in supernatants of Cab45KO cells after 2 and 4 h of secretion. The mean fold-change is about 2.3-fold higher after 4 h (*; $p= 0.1257$) and about 1.4-fold higher after 2h ($p= 0.2018$) of secretion in pulldown from

Cab45KO compared to HeLa cell supernatant. Statistical analysis was performed using t-test (confidence level 87%) in GraphPad Prism 7. (* $p<0.13$, ** $p<0.013$, *** $p<0.001$)

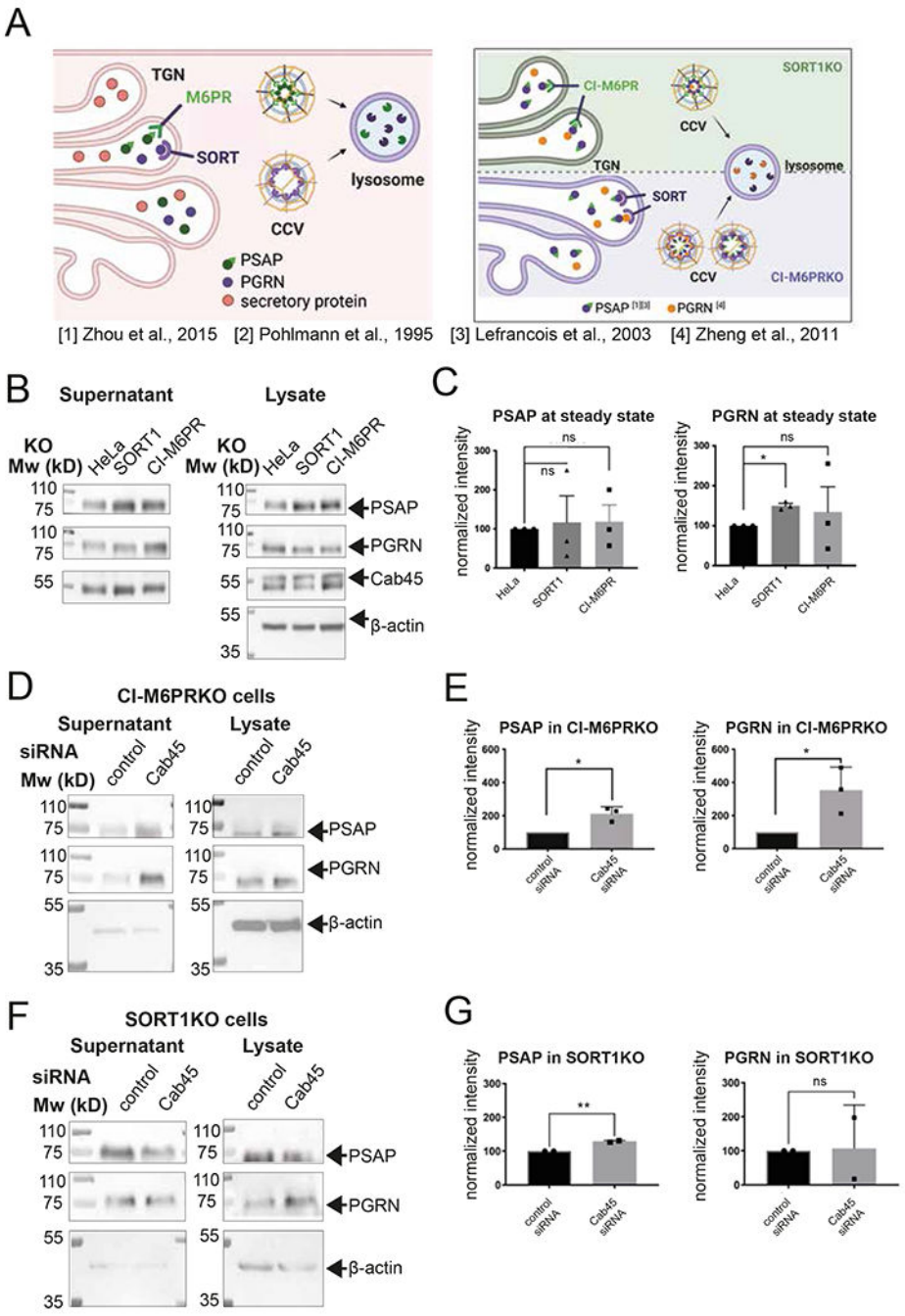

Figure 3. Cab45 depletion in M6PRKO cells enhances PSAP secretion.

(A) Scheme of the sorting action of lysosomal hydrolase receptors in the TGN, highlighting the ability of PSAP to use both M6PR and SORT1 receptors in wild-type, CI-M6PRKO, and SORT1KO conditions. **(B)** Immunoblotting of lysates and secreted proteins from HeLa, CI-M6PRKO, and sortilin knockout (SORT1KO) cells at steady state. PSAP secretion is increased in CI-M6PRKO and SORT1KO supernatants compared to HeLa cells. PGRN secretion increases in SORT1KO supernatant compared to HeLa and CI-M6PRKO cells. **(C)** Densiometric quantification of the western blot in **B** for PSAP and PGRN of three

independent experiments show nonsignificant differences in normalized intensity of western blot signals for PSAP in CI-M6PRKO and SORT1KO. In contrast, normalized intensity is significantly increased for PGRN (*. p = 0.0126) in SORT1KO supernatants. **(D)** Induction of hypersecretion phenotype for PSAP in CI-M6PRKO cells after treatment with Cab45 siRNA. **(E)** Increased PSAP secretion indicated is quantified by densitometry of western blots of three independent experiments from **D** as significantly different in comparison with control siRNA-treated CI-M6PRKO cells (PSAP:*, p = 0.0103; PGRN: *, p = 0.0342). Error bars show the SD of normalized intensity of western blot bands in %. **(F)** Secretion assay using the same conditions described in **D** in SORT1KO cells after Cab45 siRNA treatment. PSAP levels are significantly increased (**, p = 0.0064), while PGRN levels are not significantly increased after Cab45 depletion of SORT1KO cells shown in immunoblot **F** or densitometry quantification of the western blot bands **(G)**. Statistical analyses were performed using t-test (confidence level 95%) in GraphPad Prism 9. (* $p<0.05$, ** $p<0.005$, *** $p<0.001$).

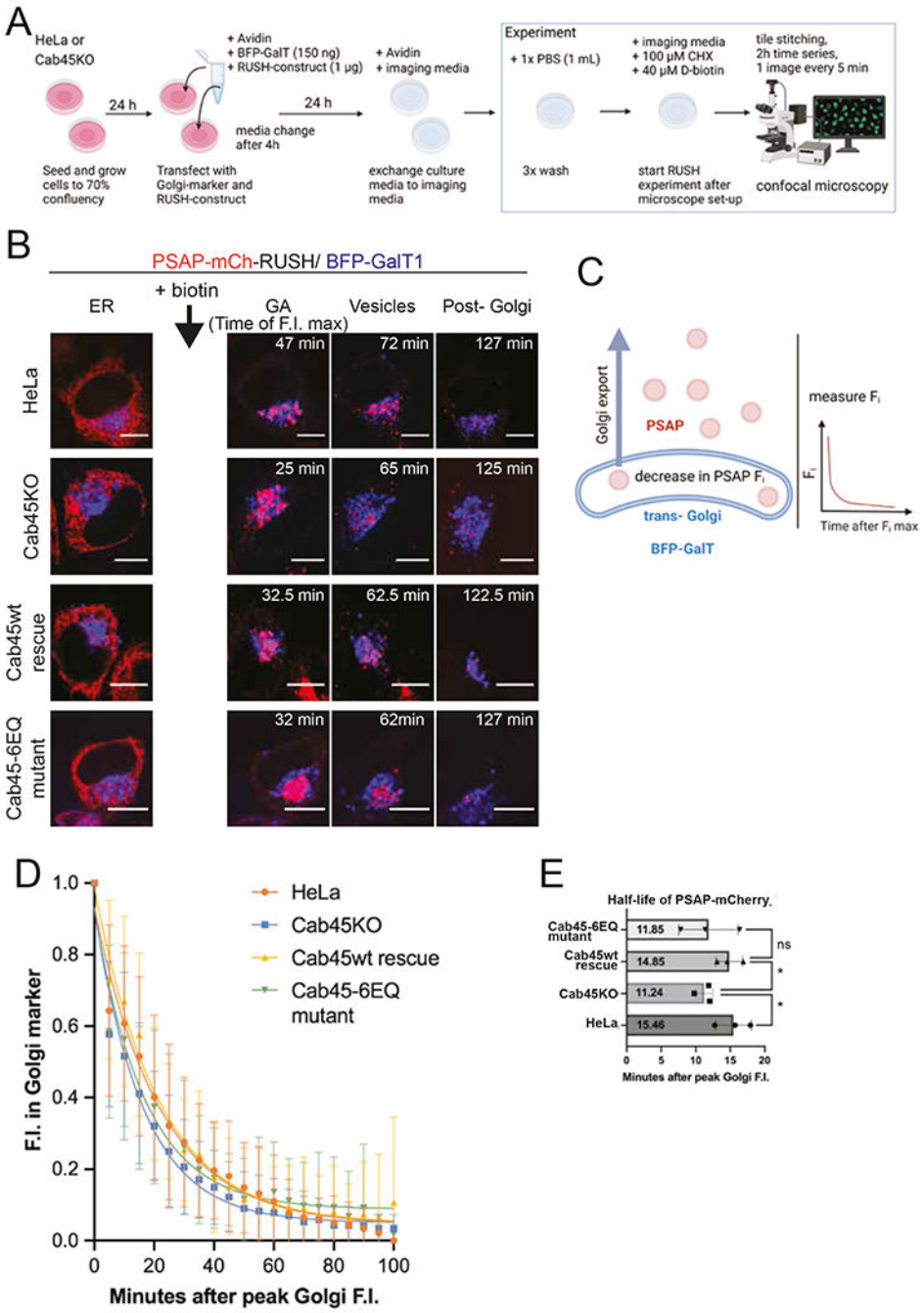

Figure 4. Visualization of PSAP trafficking using RUSH indicates increased trans-Golgi exit in Cab45KO cells in live-cell imaging.

(A) Workflow for RUSH system combined with live-cell imaging with trans-Golgi marker BFP-GalT1 in HeLa and Cab45KO cells as trans-Golgi exit assay. **(B)** Confocal micrographs of the RUSH assay in live-cell-imaging to study the trans-Golgi exit of RUSH PSAP-mCherry in HeLa vs. Cab45KO, Cab45wt rescue, and Cab45-6EQ mutant cells showing fluorescence for indicated time points after biotin addition. RUSH PSAP-mCherry is localized in the ER, then reaches peak F.I. in the trans-Golgi (GA), the measured starting

point of the trans-Golgi exit **(C)**. The scheme illustrates the decay of the PSAP F.I. (red circles) in the region overlapping with the trans-Golgi marker (BFP-GalT). An exponential curve illustrates protein exit. **(D)** Protein exit is depicted as exponential decay curves. Graph depicting mean normalized fluorescence intensity (F.I.) of RUSH PSAP-mCherry in BFP-GalT1 (trans-Golgimarker) region of interest (ROI) from and after the time when the maximal PSAP-mCherry F.I. is reached in the ROI (peak Golgi F.I.). The decrease in PSAP-mCherry F.I. represents the trans-Golgi exit in HeLa (orange) versus Cab45KO (blue), Cab45wt-rescue (yellow), and Cab45-6EQ mutant (green) cells. At least 50 cells from three independent experiments for each condition were analyzed with nonlinear regression (exponential function) indicated in the plot using GraphPad Prism9 built-in regression. **(E)** The half-life of RUSH PSAP-mCherry is shown as the time when the reduction in F.I. decreased to 50% of the peak F.I. The half-life was calculated by using a One-phase-decay exponential curve analysis. P-values were calculated using t-test (confidence level 90%) in GraphPad Prism 9. (* $p<0.1$, ** $p<0.01$, *** $p<0.001$).

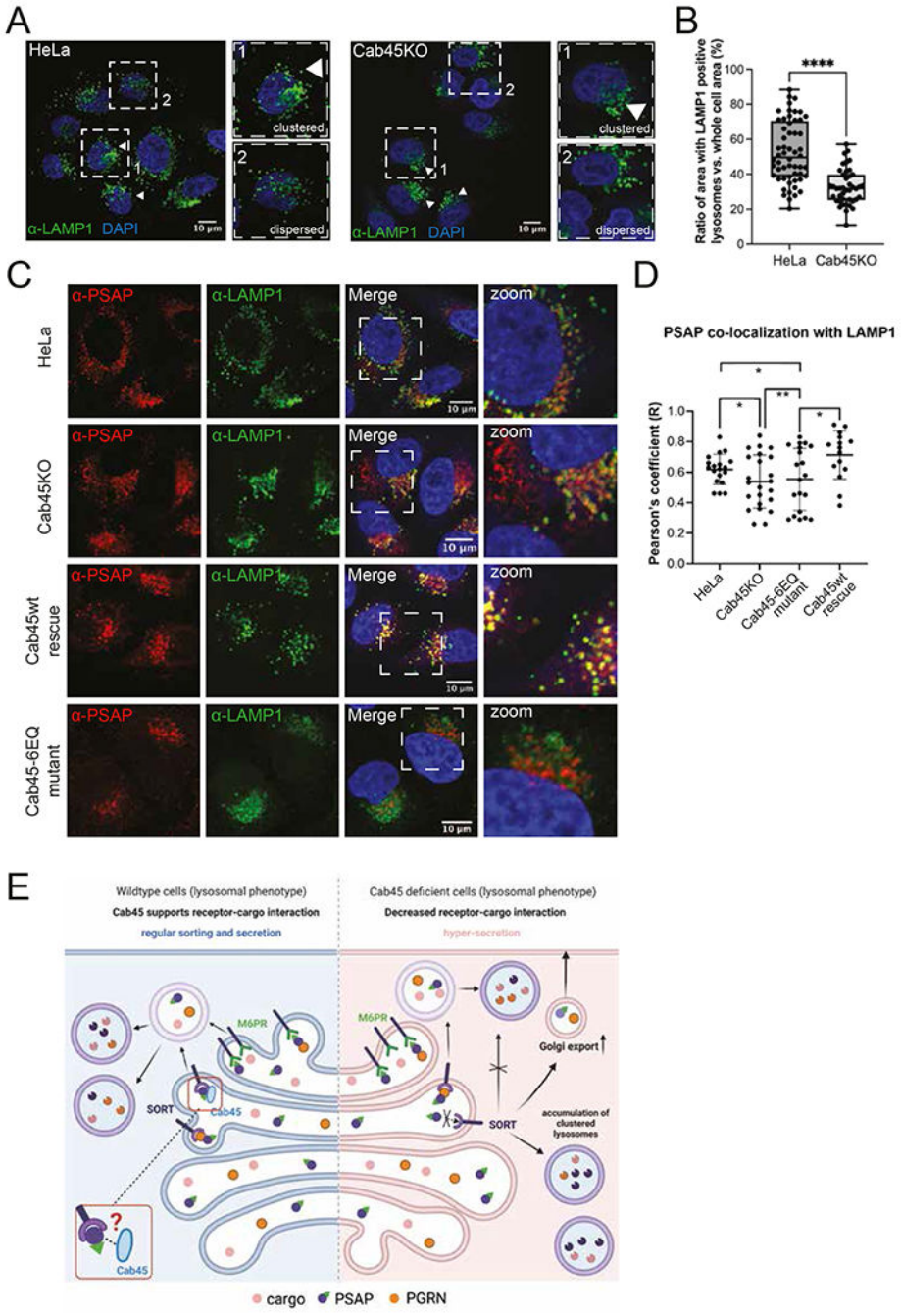

Figure. 5. Cab45 deficiency leads to aberrant perinuclear accumulation of LAMP1-positive lysosomes.

(A) The two observed phenotypes of lysosomal organization with accumulated (1) and dispersed (2) LAMP1 localization are shown in representative images and quantified by calculating the area of LAMP1 to the whole cell area in the box plot, scale bar 10 μm; **(B)** Plot shows a higher number of cells with peripheral lysosomes for HeLa with a mean area coverage of LAMP1 of 52.43% (56 cells). For Cab45KO cells, the trend was reversed, with more frequent perinuclear localized lysosomes having a mean coverage of 33.37% (42

cells). Kruskal-Wallis statistics revealed a highly significant difference between the area coverage of LAMP1 per cell. Error bars show the highest and lowest values with 5%-95% percentile indicated as boxes. **** $p<0.0001$; **(C)** Representative images of LAMP1 (green) and PSAP (red) in control HeLa, HeLa Cab45KO, HeLa Cab45KO line expressing Cab45-6EQ mutant and HeLa Cab45KO line expressing Cab45wt (rescue experiment) cells depict PSAP co-localizing with LAMP1-positive structures, scale bar 10 μm. **(D)** The graph depicts the quantification of PSAP overlapping with LAMP1 using Pearson's coefficient defining "1" as 'perfect co-localization, show Cab45KO and Cab45-6EQ mutant cells with lower co-localization compared to HeLa and cells and rescued with Cab45wt. Statistical analysis was performed with 15-23 cells from 3 independent experiments and revealed significant differences for HeLa vs. Cab45KO (*, $p = 0.0846$), HeLa vs. Cab45-6EQ mutant (*, $p = 0.0416$), Cab45-6EQ vs. Cab45wt rescue (*, $p = 0.0177$) and highly significant differences for Cab45KO vs. Cab45-6EQ mutant (**, $p = 0.0036$). P-values were calculated using t-test (confidence level 90%) in GraphPad Prism 9. (* $p<0.1$, ** $p<0.01$, *** $p<0.001$). (**E**) Proposed model of sorting of lysosomal proteins in wild-type (left) and Cab45 deficient cells (right). Under wild-type conditions, Cab45 might support the receptor-cargo interaction of sortilin (depicted as zoom). Lysosomal proteins PSAP and PGRN can be recognized and bound by their receptors and sorted into endolysosomal structures (light red circle) before maturing to their processed forms in lysosomes (purple circle). Results from this study indicate that in Cab45 deficient cells, the recognition of sortilin and its cargo is decreased, leading to increased trans-Golgi export and secretion of immature lysosomal protein PSAP (hypersecretion). PSAP can be partially sorted by the interaction with PGRN to the endolysosomal route.